


Hydrodynamic effects in kinetics of phase separation in binary fluids: Critical versus off-critical compositions

Koyel Das and Subir K. Das *

Theoretical Sciences Unit and School of Advanced Materials, Jawaharlal Nehru Centre for Advanced Scientific Research, Jakkur, Bangalore 560064, India



(Received 10 February 2022; accepted 28 March 2023; published 21 April 2023)

Via hydrodynamics-preserving molecular dynamics simulations we study growth phenomena in a phase-separating symmetric binary mixture model. We quench high-temperature homogeneous configurations to state points inside the miscibility gap, for various mixture compositions. For compositions at the symmetric or critical value we capture the rapid linear viscous hydrodynamic growth due to advective transport of material through tubelike interconnected domains. For state points very close to any of the branches of the coexistence curve, the growth in the system, following nucleation of disconnected droplets of the minority species, occurs via a coalescence mechanism. Using state-of-the-art techniques, we have identified that these droplets, between collisions, exhibit diffusive motion. The value of the exponent for the power-law growth, related to this diffusive coalescence mechanism, has been estimated. While the exponent nicely agrees with that for the growth via the well-known Lifshitz-Slyozov particle diffusion mechanism, the amplitude is stronger. For the intermediate compositions we observe initial rapid growth that matches the expectations for viscous or inertial hydrodynamic pictures. However, at later times these types of growth cross over to the exponent that is decided by the diffusive coalescence mechanism.

DOI: [10.1103/PhysRevE.107.044116](https://doi.org/10.1103/PhysRevE.107.044116)

I. INTRODUCTION

When quenched inside the coexistence region, a homogeneously mixed binary (A + B) system separates into phases that are rich in A and B particles [1–10]. This transformation occurs via formation and growth of domains of like particles. Such an evolution process is complex, during which the evolving structure exhibits interesting self-similar properties [2,4–7]. The latter implies that the structures at two different times are the same, except for the difference in size. As a consequence, one observes the scaling behavior [2,6]

$$C(r, t) \equiv \tilde{C}(r/\ell(t)) \quad (1)$$

of the two-point equal-time correlation function [2,6]

$$C(r, t) = \langle \psi(\vec{r}_1, t) \psi(\vec{r}_2, t) \rangle - \langle \psi(\vec{r}_1, t) \rangle \langle \psi(\vec{r}_2, t) \rangle, \quad (2)$$

$\tilde{C}(x)$ being a master function that is independent of time. In Eqs. (1) and (2), $r = |\vec{r}_1 - \vec{r}_2|$, $\ell(t)$ represents the average size of domains at time t , and ψ is a space- and time-dependent order parameter, that can be defined as the local concentration difference between the two species [10–12]. Typically, ℓ grows in a power-law fashion as [2,4–7]

$$\ell \sim t^\alpha. \quad (3)$$

The growth exponent α depends upon several parameters [2,7]. In a nonhydrodynamic environment, one expects $\alpha = 1/3$. This is referred to as the Lifshitz-Slyozov (LS) growth law [8,13–19] and is a result of diffusive transport of particles,

via a chemical potential gradient. The LS picture applies to phase-separating solid mixtures and remains valid for critical as well as off-critical compositions [8], for the entire growth period. In fluids, however, hydrodynamics is important. There the mechanisms and exponents are different for the above two situations that give rise, respectively, to bicontinuous and disconnected droplet morphologies [20–43]. This is true for vapor-liquid as well as liquid-liquid transitions, in the former case density playing the role of composition. Please note that the LS mechanism not only is applicable to solid solutions but also applies to liquids. For example, irrespective of the composition in a phase-separating liquid mixture, the early-time dynamics can be dominated by this mechanism. Below we briefly describe the hydrodynamic picture in the liquid-liquid context.

Consider a composition close to the critical value, say, a 50 : 50 proportion of A and B particles for a symmetric model of a mixture. In this case [6,7,10,22–24] the systems become unstable owing to small fluctuations, and the phase separation occurs via formation of elongated percolating domains of both the species. Fast advective transport of material, in the presence of hydrodynamics, is expected to occur through these tubelike channels, having undulating domain boundaries, due to the pressure gradient related to the interfacial tension [22–24]. Overall growth in this situation is not described by a single exponent. At very early times the LS picture remains valid [6,7]. Following this hydrodynamics becomes important, leading to a crossover of the exponent to $\alpha = 1$, in space dimension $d = 3$, which is referred to as the viscous hydrodynamic growth [6,7,10,22,35,38]. At an even later time a further crossover occurs to a smaller value, viz.,

*das@jncasr.ac.in

$\alpha = 2/3$, known as the inertial hydrodynamic exponent [6,7]. These two growth exponents can be obtained by balancing the interfacial free energy density with viscous stress and kinetic energy density, respectively.

For a composition very close to any of the branches of the coexistence curve, on the other hand, the growth, in a hydrodynamic environment, may occur via coalescence of disconnected droplets that consist primarily of particles of the minority phase [20–22,29–31,33,38,43]. Such a picture was proposed by Binder and Stauffer [20], Binder [21], and Siggia [22] (herein referred to as the BS mechanism). For diffusive motion of the droplets, between collisions, which is a possibility for liquid mixtures, because of the high-density background phase, solution of the dynamical equation [22]

$$\frac{dn}{dt} = -D\ell n^2, \quad (4)$$

for droplet density n ($\propto 1/\ell^d$), provides $\alpha = 1/d$. In Eq. (4), D is a diffusion constant, having dependence upon ℓ . It is expected that $D\ell$ will remain a constant, during the growth period, in accordance with the generalized Stokes-Einstein-Sutherland [44–46] relation. In $d = 3$, the BS value is the same as the LS exponent. The difference in the mechanisms is expected to be captured in the amplitudes of growth, the latter being larger for the BS case. The ratio of the amplitudes for the two mechanisms is supposed to follow the relation [33]

$$\frac{A_{BS}}{A_{LS}} = K\phi^{1/3}, \quad (5)$$

where K is a constant ($\simeq 6$) and ϕ is the volume fraction of the minority species in the mixture. Note here that other types of droplet motions, viz., subdiffusive and superdiffusive, cannot be straightforwardly discarded.

In this paper, we present results for a wide range of compositions. We report how the growth law depends upon the overall composition in a hydrodynamic environment. Our results were obtained via molecular dynamics (MD) [47,48] simulations. Even though the above-discussed picture is for binary fluids [6,20–24], morphology-dependent systematic simulations of atomistic models exist only for the vapor-liquid transition [49]. In our canonical ensemble simulations the temperature is controlled via the Nosé-Hoover thermostat (NHT) [47,50–52]. The latter is known to preserve hydrodynamics. The obtained results were analyzed via appropriate methods to arrive at conclusions as to the growth and mechanism.

The rest of the paper has been arranged as follows. We describe the model and methods in Sec. II. Section III contains the results. We conclude the paper in Sec. IV with a brief summary.

II. MODEL AND METHODS

In our model system, two particles, located at \vec{r}_i and \vec{r}_j , with $r = |\vec{r}_i - \vec{r}_j|$, interact via the potential [48]

$$U(r) = V(r) - V(r_c) - (r - r_c) \left[\frac{dV(r)}{dr} \right]_{r=r_c}, \quad (6)$$

for $r < r_c$, the latter being a cutoff distance. In Eq. (6), $V(r)$ is the standard Lennard-Jones (LJ) potential [48]

$$V(r) = 4\epsilon_{\alpha\beta} \left[\left(\frac{\sigma_{\alpha\beta}}{r} \right)^{12} - \left(\frac{\sigma_{\alpha\beta}}{r} \right)^6 \right]. \quad (7)$$

The term $V(r_c)$, on the right-hand side of Eq. (6), cuts and shifts the potential (to zero) at $r = r_c$. While this is beneficial for computation, the procedure leaves the force discontinuous at r_c . The other additional term, viz., $(r - r_c)dV(r)/dr|_{r=r_c}$, removes this discontinuity [48]. In Eq. (7), $\epsilon_{\alpha\beta}$ and $\sigma_{\alpha\beta}$, $\alpha, \beta \in [A, B]$, represent the interaction strengths and diameters, respectively, for various combinations of particles.

Here, $\sigma_{\alpha\beta}$ and $\epsilon_{\alpha\beta}$ among the like particles are taken to be the same; namely, we have $\sigma_{AA} = \sigma_{BB} = \sigma$ and $\epsilon_{AA} = \epsilon_{BB} = \epsilon$. We also choose $\sigma_{AB} = \sigma$. In that case, to facilitate phase separation, one must fix ϵ_{AB} in such a way that like particles tend to gather; that is, one should have $\epsilon_{AB} < \epsilon$. We consider $\epsilon_{AB} = \epsilon/2$. Thus we have [53]

$$\sigma_{AA} = \sigma_{BB} = \sigma_{AB} = \sigma \quad (8)$$

and

$$\epsilon_{AA} = \epsilon_{BB} = 2\epsilon_{AB} = \epsilon. \quad (9)$$

We have also set the mass m of all the particles to be equal. Thus our model is perfectly symmetric. This provides an Ising-like situation that has been very useful in studying the kinetics of phase separation.

Due to the established utility of the model for studies of phase separation in fluid systems, as well as to exploit the previous results [10,53,54] as good references, we choose this model for the present study. This is also meaningful by considering that we do not expect any model-dependent hydrodynamic behavior as far as scaling aspects in growth and structure are concerned. For this *symmetric* model, the phase diagram, in $d = 3$, is accurately known for (number) density of particles $\rho = 1$. It is, of course, expected [53,54] that the critical concentration, for any of the species, will be $x_\alpha^c = 1/2$. Note that the concentration of a species within the mixture is defined as $x_\alpha = N_\alpha/N$, N_α being the number of particles of type α and $N = N_A + N_B$. The critical temperature T_c was estimated to be $\simeq 1.421\epsilon/k_B$, where k_B is the Boltzmann constant [53,54]. The coexistence curve is shown in Fig. 1. In this diagram the results for a finite number of particles ($N = 7200$) [53,54] were obtained via Monte Carlo simulations [55] in a semi-grand-canonical ensemble.

In the following we set σ , ϵ , m , and k_B to unity. In this paper we study the kinetics via MD by quenching homogeneous configurations, prepared at a high temperature, to the temperature $T = 1$. The compositions are chosen in such a way that the final-state points fall inside the miscibility gap [53,54]. Those state points are marked inside the coexistence curve of Fig. 1.

We have performed MD simulations [47] in periodic cubic boxes of linear dimension L , the latter being measured in units of σ . As already stated, the temperature was controlled via the application of a NHT [47,50–52] that is known to preserve hydrodynamics well. Note that the hydrodynamics is well satisfied during MD simulation in a microcanonical ensemble. However, during phase separation, such a constant-energy method is not advisable. This will lead to shift in temperature

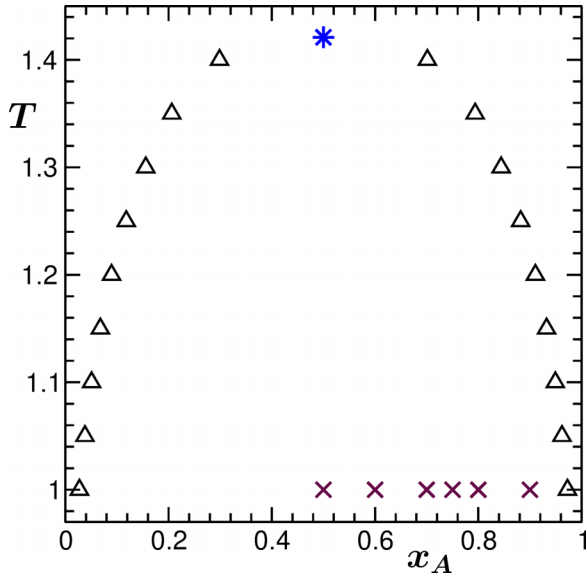


FIG. 1. Phase coexistence curve for the symmetric LJ binary mixture with overall density 1 in the T vs x_A ($= N_A/N$) plane. These simulation data, represented by the triangles, were obtained via Monte Carlo simulations in a semi-grand-canonical ensemble with 7200 particles. The asterisk represents the critical point of the system that was obtained earlier [53,54] via appropriate analysis. The crosses correspond to the state points to which the systems were quenched.

to values above the coexistence curve where A and B components will be mixed. Thus constant-temperature methods are necessary. For the latter purpose, all available thermostats do not satisfy the requirements of hydrodynamics. For example, hydrodynamics is ignored in the Andersen thermostat (AT) [47,56], which operates via a stochastic mechanism.

Many works report results [10,11,38], by using an NHT, that produce key expectations for hydrodynamic behavior in the kinetics of phase separation. In this connection, we draw attention to Ref. [57]. In that work, in the equilibrium context, results for various transport properties in fluids were compared from the calculations in canonical (with an NHT) and microcanonical ensembles. Recall that in the latter ensemble the hydrodynamics is perfectly satisfied. It was observed that except for bulk viscosity, results for other transport coefficients were in good agreement from the two ensembles. Given that we are dealing with a nearly incompressible fluid, bulk viscosity is less relevant. Thus application of the NHT is rather safe here.

It is worth mentioning here that MD simulations for the kinetics of phase separation in binary fluids are difficult. Here, to avoid the effects of a vapor-liquid transition, one needs to deal with high overall density. This restricts the system size and, thus, access to large length scales. The problem becomes significantly more severe for compositions close to the coexistence curve. Because of this, the droplet growth aspect, though important, did not receive attention.

In our MD method we have used the Verlet velocity integration scheme [47,48], with time discretization step $\Delta t = 0.001\tau$. Here, τ ($= \sqrt{m\sigma^2/\epsilon}$) is our LJ unit of time, which is unity because of the abovementioned choices of ϵ , σ , and

m . All our quantitative results are presented after averaging over runs with a minimum of 50 independent initial configurations. Unless otherwise mentioned, all the simulations were performed with $L = 64$.

We have calculated lengths from the decay of the correlation function as

$$C(r = \ell, t) = c, \quad (10)$$

by fixing c to the first zero of the correlation function. It is worth mentioning here that for conserved order-parameter dynamics, the class to which the present problem belongs, C exhibits damped oscillations around zero. This we will see in the next section. For the calculation of $C(r, t)$ we have mapped the continuum configurations to the ones on a simple cubic lattice [8]. Details on this and the estimation of local order parameter are provided later. The length was also obtained by direct identification of the droplets [58] and counting numbers of particles within those [49]. The latter, of course, provides a quantity proportional to volume, from which the average length can be trivially obtained following calculation of the average volume via the first moment of a distribution. Results from different methods are essentially proportional to each other, differing by constant factors.

For a disconnected morphology, the droplet identification [58] is important for the purpose of confirmation of the mechanism as well, e.g., via the calculation of mean-square displacement (MSD) of the centers of mass (CMs) of the droplets. Note that for N_p particles belonging to a particular droplet the center of mass is calculated as [44]

$$\vec{R}_{\text{CM}}(t) = \frac{1}{N_p} \sum_{i=1}^{N_p} \vec{r}_i(t). \quad (11)$$

The MSD is then obtained from the formula [44]

$$\text{MSD} = \langle (\vec{R}_{\text{CM}}(t') - \vec{R}_{\text{CM}}(0))^2 \rangle. \quad (12)$$

Here, t' is a time that is shifted with respect to the time at the beginning of an observation.

III. RESULTS

In Fig. 2 we show snapshots taken during the evolutions of two typical homogeneously mixed configurations towards respective equilibria, following quenches inside the coexistence curve. For the 50 : 50 composition, it is appreciable that the morphology consists of interconnected tubelike domains. For the asymmetric composition, disconnected droplet morphology is clearly identifiable. While the spherical structure can be appreciated from the snapshots, we have confirmed it via the calculation of radius of gyration as a function of mass. In the disconnected case the growth seems to be much slower. Our objective here is to provide a composition-dependent quantitative picture.

In Fig. 3 we show scaling exercises [6] for the correlation function. There, $C(r, t)$ is plotted versus r/ℓ . Results from a few different times, for two compositions, have been included. Figure 3(a) contains results for the symmetric composition, and the results for the 90 : 10 composition are included in Fig. 3(b). The nice collapse of the data sets implies self-similarity of growth in both of the cases. For conserved

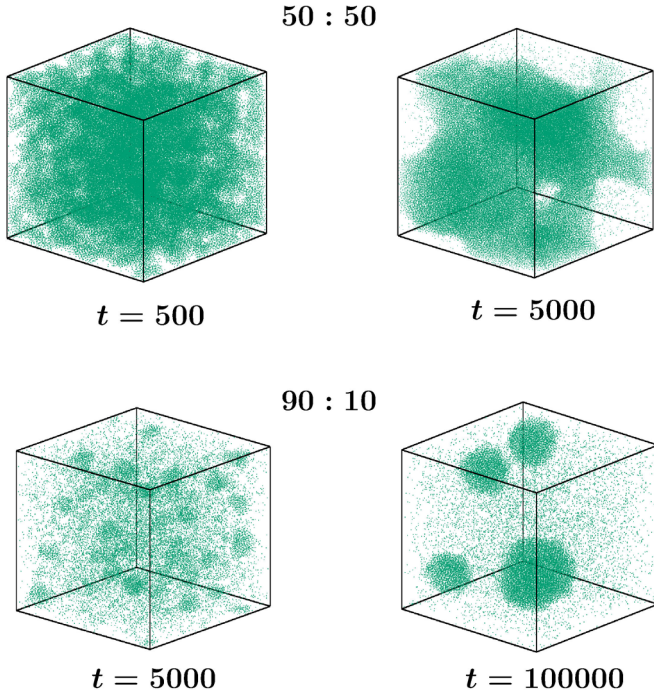


FIG. 2. Snapshots, which were recorded during the molecular dynamics simulations, following quenches of high-temperature homogeneous configurations to $T = 1$, are shown for 50 : 50 (top) and 90 : 10 (bottom) compositions of A and B particles. Only the locations of the B particles are marked. For each of the compositions, frames from two different times are included.

order-parameter dynamics, one expects damped oscillations of $C(r, t)$ around zero. This is clearly visible here. In the asymmetric composition case the minimum is expectedly much shallower compared with the symmetric or critical (50 : 50) composition case [59].

In the insets of Fig. 3 we show the scaling plots of $S(k, t)$, the structure factor, a quantity that is of direct experimental relevance [6]. This is the Fourier transform of $C(r, t)$. The expected scaling form for this quantity is [6]

$$S(k, t) \equiv \ell^d \tilde{S}(k\ell), \quad (13)$$

where $\tilde{S}(y)$ is another time-independent master function. Clearly, good collapse of data from different times is visible. The small- k behavior is consistent with k^4 [10,59], for the symmetric case, referred to as the Yeung's law [60]. The result for the asymmetric case, however, is at deviation [59] with the Yeung's law. This possibly is an artifact of off-critical composition. It may as well be true that the k^4 behavior [60] will be realized in the asymptotically large droplet size limit. This, however, is difficult to confirm via simulations and is not our objective here. The large- k behavior is consistent with a power law having an exponent -4 , in both of the cases. This is the expected Porod law [61–63] in $d = 3$, for a scalar order parameter, and is an outcome of scattering from sharp interfaces. The deviations that are observed can be due to the interfacial roughness that is appreciable from the noise that is noticed in the snapshots of Fig. 2. Such noise can be gotten rid of via choices of lower quench temperatures. This may, however, lead to undesirable situations. For example, crystallization is a possibility. In this paper, for the purpose

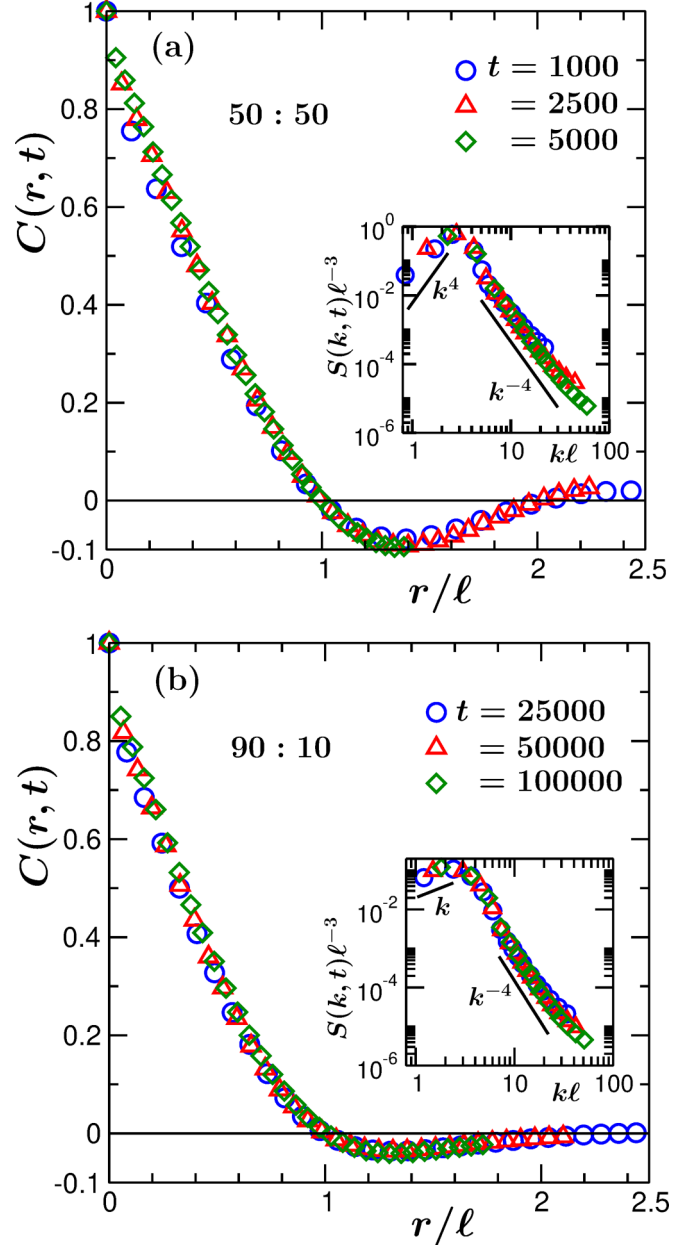


FIG. 3. (a) Two-point equal-time correlation functions, $C(r, t)$, are shown, from a few different times, vs the scaled distance $r/\ell(t)$, for a 50 : 50 composition. In the inset we show the analogous scaling plots for the structure factor, $S(k, t)$, k being the wave number. The solid lines in the inset represent power laws. (b) Same as (a), but here the composition is 90 : 10.

of analysis, this noise was largely eliminated via the application of a majority rule [8]. In this method, at the location of each particle we have calculated the concentration difference between the two species, by considering a neighborhood of radius σ . If it is positive, we have assigned a value of $+1$, otherwise -1 , to the order parameter as in the Ising model. Prior to this calculation we have appropriately mapped each continuum configuration to a lattice one with lattice constant σ . Before moving to the discussion on growth, we mention that ℓ can be estimated from the first moment of $S(k, t)$ as well [6].

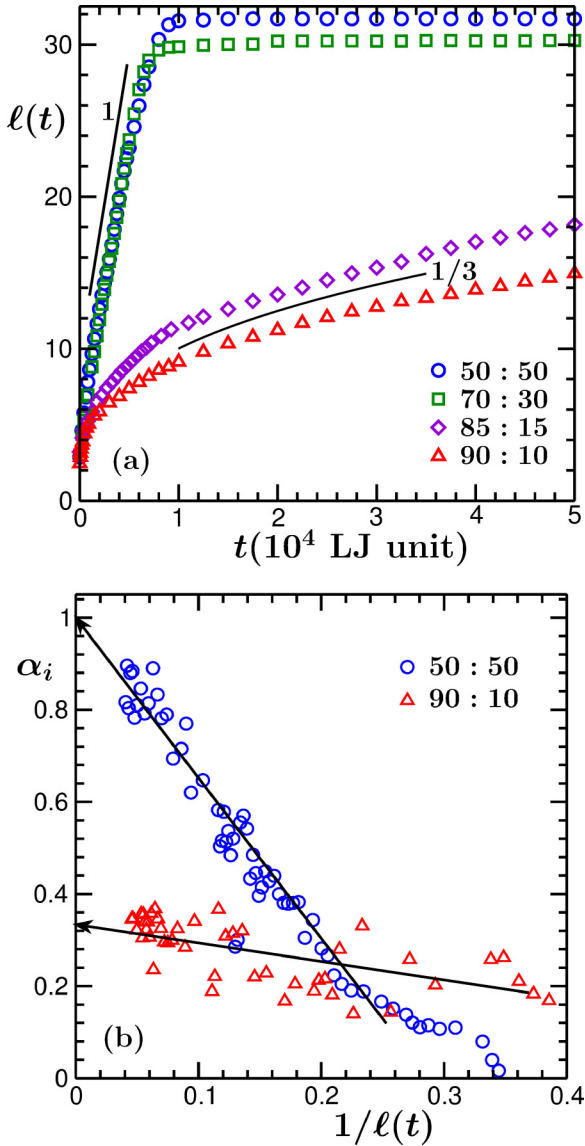


FIG. 4. (a) Average domain lengths, $\ell(t)$, are shown with the variation of time, for quenched systems having different compositions of A and B particles. The solid lines represent power laws with the given exponents. (b) Instantaneous exponents are shown as a function of $1/\ell$, for the compositions 50 : 50 and 90 : 10. The long arrows there are guides to the eye.

In Fig. 4(a) we show ℓ versus t plots for several different compositions. For compositions at or close to the symmetric value, the intermediate-time behavior, over long periods, is linear, consistent with the expectation for viscous hydrodynamic growth. The saturations at late times are due to the finite size of the systems. Note that the maximum domain length is less than the system size. This is because two phases occupy the box. The late-time behavior, for compositions far away from the critical value, is consistent with $\alpha = 1/3$. This is expected for the BS [20–22] mechanism, in $d = 3$. For a more convincing confirmation of the values of the exponents, we have calculated the time-dependent or instantaneous exponent [8,16,17] $\alpha_i (= d \ln \ell / d \ln t)$. This quantity is shown in Fig. 4(b) for 50 : 50 and 90 : 10 compositions, with the

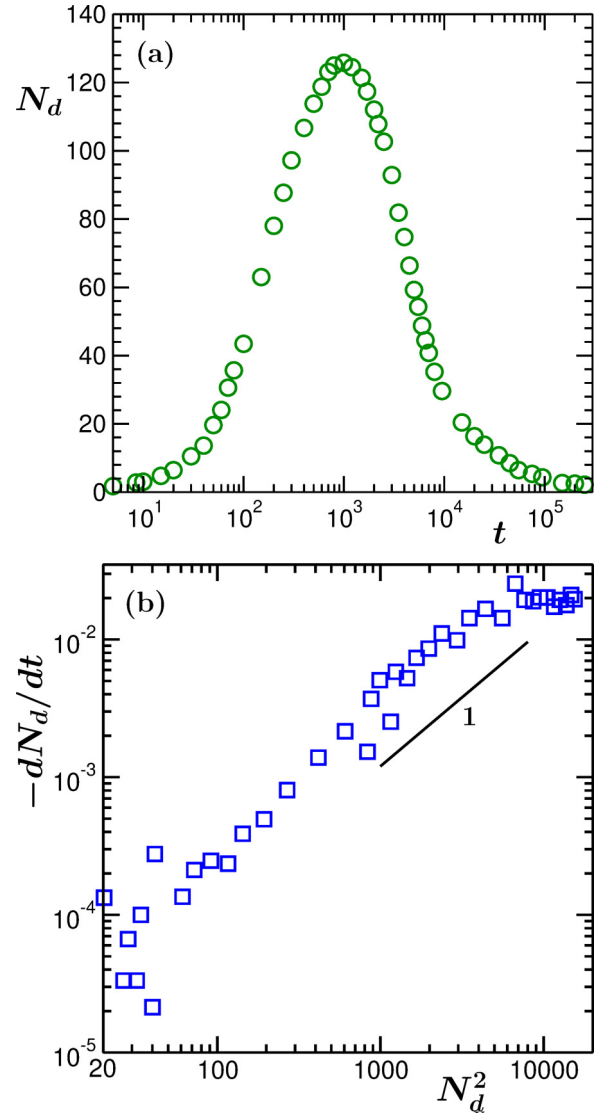


FIG. 5. (a) Here we have plotted the number of droplets, consisting primarily of the particles of the minority phase, as a function of time, on a semilog scale, for 90 : 10 composition. (b) A plot of $-dN_d/dt$ vs N_d^2 , on a log-log scale, corresponding to the plot in (a). The solid line is a power law with exponent 1.

variation of $1/\ell$. If ℓ is written as $\ell = \ell_0 + At^\alpha$, ℓ_0 being the length at the beginning of scaling and A being the growth amplitude, then α_i should follow [8,17]

$$\alpha_i = \alpha[1 - \ell_0/\ell].$$

When plotted versus $1/\ell$, it appears from the above equation that the data for α_i will exhibit a linear behavior with slope $-\alpha\ell_0$ and ordinate intercept α . For both the compositions the simulation data in Fig. 4(b) are consistent with this picture, implying $\alpha = 1$ and $1/3$, for the respective compositions. Having identified the exponent for the power-law growth for the off-critical case, we present results that will ascertain that the growth indeed occurs via the diffusive coalescence mechanism.

In Fig. 5(a) we present a plot for the number of droplets (N_d) as a function of time. The early part is dominated by

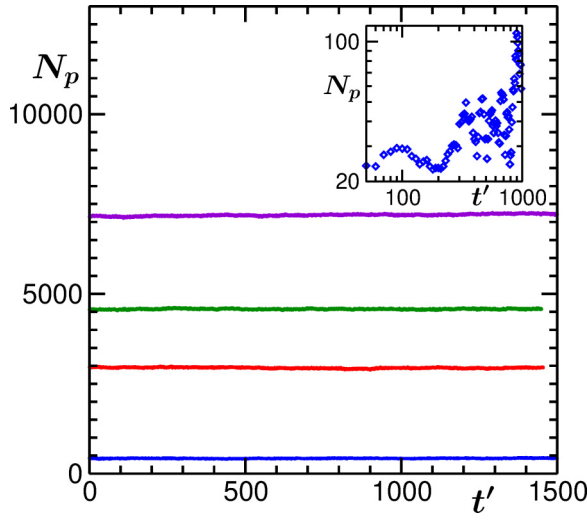


FIG. 6. Numbers of particles, N_p , in a few droplets, are shown as a function of the translated time $t' = t - t_0$, t_0 being the beginning of an observation. These results are for the composition 90 : 10 and $L = 48$. During the presented periods the considered droplets did not undergo collision with other droplets. The inset shows a similar plot for a droplet from the early nucleation period.

nucleation. The late-time decay is due to growth. In Fig. 5(b) we show a plot of $-dN_d/dt$ versus N_d^2 . There the focus is on the late-time growth part. Thus we have shown data from $t = 5000$ onward. The linear behavior on a double-log scale indicates a power law. We expect [38] an exponent 1 for diffusive coalescence; see Eq. (4) and related discussion. That indeed is observed. This also indirectly validates the Stokes-Einstein-Sutherland [44–46] relation in this extended context.

In Fig. 6 we show numbers of particles (N_p) in several droplets, with the variation of time t' that is calculated from the beginning of an observation. During the presented periods these droplets did not collide with any other droplets. In each of the cases the value of N_p remains practically constant. This again suggests that the LS-like particle diffusion mechanism [13] is playing a negligible role in the growth. The number of droplets is decreasing, as seen in Fig. 5, due to coalescence. This should be compared with the nucleation regime; see the inset of Fig. 6. During this initial stage the number of particles in a nucleus increases, via deposition of particles from the neighborhood. Due to the complex environment, occasionally particles can get detached from the droplets. Thus fluctuations can occur (as seen in the inset of Fig. 6), which may appear prominent at early times. A steady rise from the very beginning should be expected only as an average behavior.

In Fig. 7 we show results related to the motion of the centers of mass of the droplets. In Fig. 7(a) a trajectory of the CM of a typical droplet is seen. Random motion of the droplet is visible. In Fig. 7(b) we show an MSD versus time plot for such a droplet. Clearly, diffusive displacement is visible, at late times.

The above results suggest that the growth is occurring via the diffusive coalescence mechanism. We have obtained further information about this by simulating asymmetric compositions with an AT. Both the NHT and the AT provide $\alpha =$

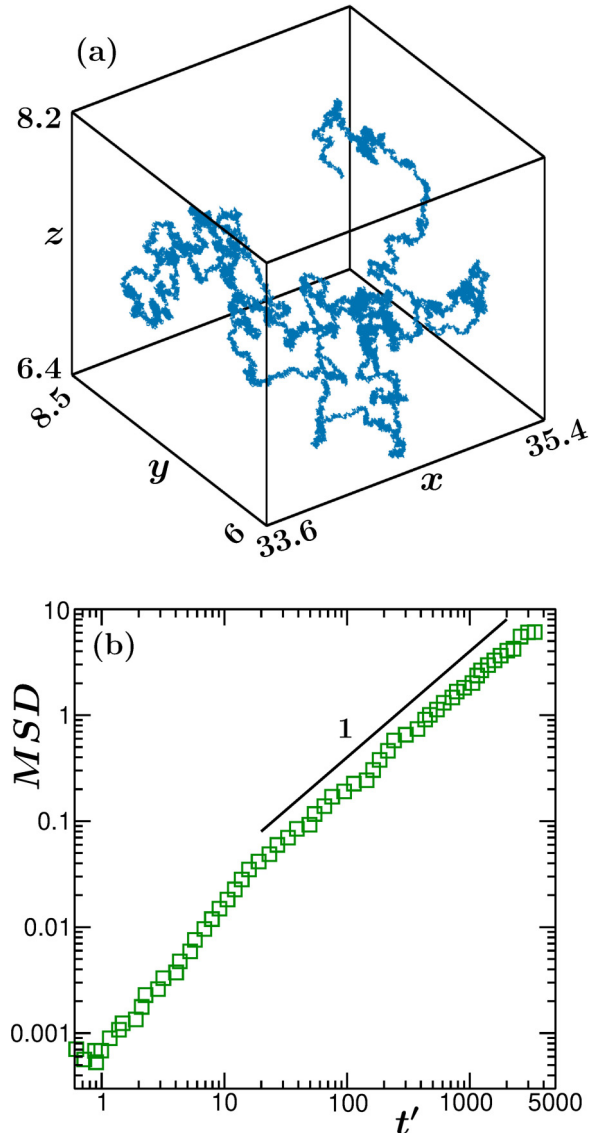


FIG. 7. (a) Here we show a trajectory of the center of mass of a typical droplet. (b) Log-log plot of the mean-square displacement (MSD) of a droplet, as a function of the shifted time t' . During this period the droplet did not encounter any collision with other droplets. The solid line represents the diffusive displacement. These results are for the composition 90 : 10.

$1/3$, in this dimension, for off-critical composition, but for different mechanisms, the LS mechanism being the case for the latter. The hydrodynamic effect is not expected for the AT. Thus the NHT should provide faster evolution, even though the exponent in both of the cases should be the same. We have checked this for an 80 : 20 composition. It indeed appears that A_{BS}/A_{LS} is > 1 . See Eq. (5) and related discussion. However, a proper match of this amplitude ratio with the theoretically expected number is not obtained [33]. This is due to the fact that even though the NHT provides the hydrodynamics, a perfect match of transport with natural systems cannot be expected, unless various thermostat parameters are appropriately tuned. Furthermore, with NHT there exists faster early growth, if the composition is not too asymmetric. On the other hand,

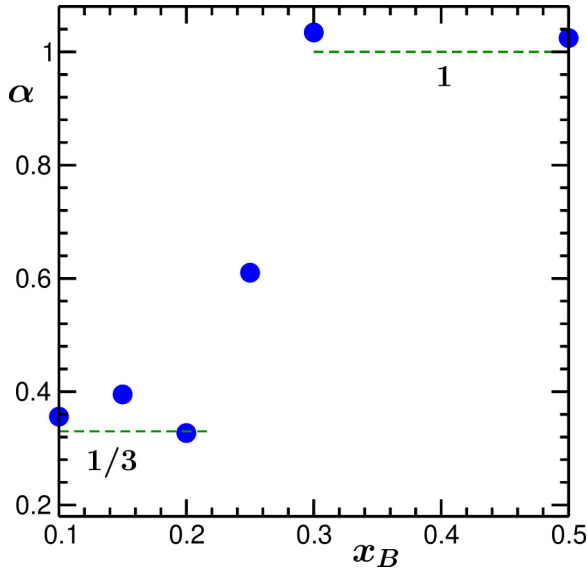


FIG. 8. Growth exponent α vs x_B . These values are obtained via extrapolations of α_i to the $\ell = \infty$ limit. The dashed lines correspond to two theoretically expected values.

simulations with the AT, for extreme off-critical compositions, are very demanding. In the following we will present more results to elucidate the abovementioned fast early growth with the NHT.

We state again that the AT was not designed to produce hydrodynamic behavior. Thus the results from this thermostat are expected to be analogous to those from the Kawasaki exchange Monte Carlo [55] simulations of the Ising model or numerical solutions of the Cahn-Hilliard (CH) equation [55], which is a continuum dynamical model. In the latter case, the order parameter remains conserved, and growth occurs via diffusive transport of material. When the CH equation is appropriately combined with the Navier-Stokes equations [6], one expects hydrodynamic behavior with faster growth. Such results have relevance in the context of outcomes from MD simulations of phase separation with NHT or other hydrodynamics-preserving thermostats.

In Fig. 8 we show a plot of α as a function of x_B , the concentration of B particles. It appears that there exist two possibilities: $\alpha = 1$ for compositions that are nearly 50 : 50 and $\alpha = 1/3$ when x_B is close to the coexistence curve, except for a very small window in the intermediate range of x_A . This window provides the impression that one is observing the inertial hydrodynamic growth here. However, we believe that this somewhat stronger than $1/3$ exponent will disappear if large systems are examined over longer periods. Here note that an inertial hydrodynamic growth is expected for interconnected morphology at very late times, past the viscous hydrodynamic evolution. See further discussion below.

In Fig. 9 we show ℓ versus t plots for quenches to all the considered state points inside the coexistence curve (see Fig. 1), on a log-log scale. For most of the compositions the early growth is faster than that provided by $\alpha = 1/3$. This may be for the following reason. During the initial period, following a quench, the domains possess an interconnected structure. Depending upon the degree of interconnectedness,

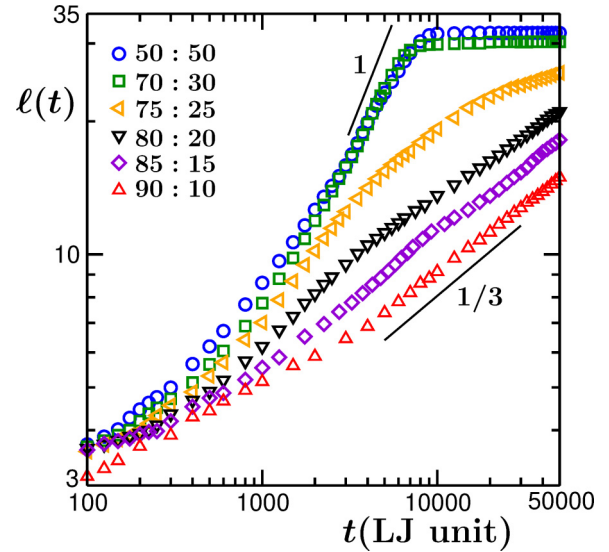


FIG. 9. Plots of $\ell(t)$ vs time, for different compositions of A and B particles, in a double-log scale. The solid lines represent power laws with the given exponents.

this may lead to various different exponents. For compositions up to 75 : 25, crossovers from stronger exponents to smaller values are clearly visible. This can be understood from the corresponding snapshots that are shown in Fig. 10. Only at late times is the disconnected structure prominent. Such a crossover will eventually happen for compositions even closer to the critical one. To realize that, we need more computational efforts.

IV. CONCLUSION

We have studied the kinetics of phase separation in a high-density symmetric binary (A + B) fluid model [48,53,54] with the variation of mixture composition. While at the symmetric composition a bicontinuous nonequilibrium domain morphology is obtained, for compositions close to a coexistence curve the domain morphology consists of disconnected droplets of the minority phase in the background of a sea consisting of particles of the majority species.

The case of a perfectly symmetric composition is much studied. In agreement with previous studies [10,22–24] we

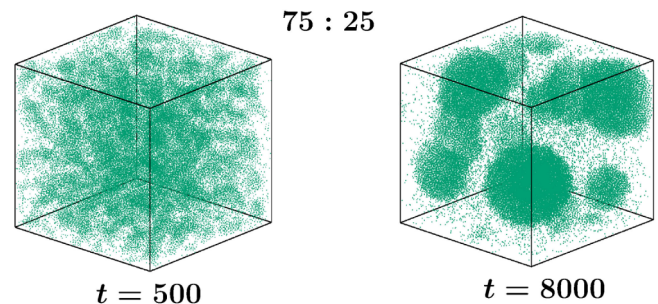


FIG. 10. Snapshots, which were recorded during the molecular dynamics simulations, following quenches of high-temperature homogeneous configurations to $T = 1$, are shown for a typical run with 75 : 25 composition of A and B particles. Only the locations of the B particles are marked.

observe a linear viscous hydrodynamic evolution within the accessible simulation length and time scales.

We have performed molecular dynamics (MD) simulations for this study. To capture the hydrodynamics, in our canonical ensemble simulations, we have used the Nosé-Hoover thermostat that is known for its capability of conservation of local momentum [47], etc. A focus of our study is on the disconnected droplet morphology. These results were discussed in the background of those obtained via the application of a stochastic Andersen thermostat [47]. Note that to study the kinetics of phase separation via MD simulation, it is necessary to use a thermostat to keep the temperature at the desired value. An alternative approach is to consider model H [6,64], which is a combination of the Cahn-Hilliard equation and the Navier-Stokes equation. This model is numerically solved on a lattice. Here our interest was in the continuum system.

We observe that the droplets are not static in the hydrodynamic environment. Via the calculation of mean-square displacements of the centers of mass, we show that these exhibit diffusive motion. Due to sticky collisions among these droplets, the number density of these objects in the system decreases, and thereby the characteristic length scale increases. For this diffusive coalescence mechanism we have accurately estimated the exponent for the power-law growth. This is in good agreement with theoretical expectations [20–22].

The picture described above is different from that obtained in a stochastic situation. In this case the droplets are practically static, and growth occurs via particle diffusion, as in solid mixtures [8,13,16,17]. The hydrodynamic growth is faster, even though the exponents in the two cases are the same.

We believe that the droplet coalescence picture is true for compositions quite close to the critical one. However, there can be faster growth until the domain structure gets disconnected through the process of saturation of domain magnetization. In this connection it may be of interest to identify the spinodal line. However, the existence of such a boundary is predicted via mean-field calculations which we do not expect to apply to the model considered here [65]. Such an exercise can be carried out for large molecular systems, such as polymers, for which the mean field is a reasonably accurate description [65,66].

ACKNOWLEDGMENTS

Parts of the simulation studies have been performed by using the Large-Scale Atomic/Molecular Massively Parallel Simulator (LAMMPS) [67,68] package. The authors acknowledge computer time at the National Supercomputing Mission located at JNCASR and partial financial support from SERB, DST, India, via Grant No. MTR/2019/001585.

-
- [1] K. Binder, *Rep. Prog. Phys.* **50**, 783 (1987).
 - [2] K. Binder, in *Phase Transformation of Materials*, edited by R. W. Cahn, P. Haasen, and E. J. Kramer (Wiley VCH, Weinheim, Germany, 1991), Vol. 5, p. 405.
 - [3] D. Kashchiev, *Nucleation: Basic Theory with Applications* (Butterworth-Heinemann, Oxford, 2000).
 - [4] R. A. L. Jones, *Soft Condensed Matter* (Oxford University Press, Oxford, 2002).
 - [5] A. Onuki, *Phase Transition Dynamics* (Cambridge University Press, Cambridge, 2002).
 - [6] A. J. Bray, *Adv. Phys.* **51**, 481 (2002).
 - [7] *Kinetics of Phase Transitions*, edited by S. Puri and V. Wadhawan (CRC, Boca Raton, FL, 2009).
 - [8] S. Majumder and S. K. Das, *Phys. Rev. E* **84**, 021110 (2011).
 - [9] S. J. Mitchell and D. P. Landau, *Phys. Rev. Lett.* **97**, 025701 (2006).
 - [10] S. Ahmad, S. K. Das, and S. Puri, *Phys. Rev. E* **85**, 031140 (2012).
 - [11] A. Singh, S. Puri, and C. Dasgupta, *J. Chem. Phys.* **140**, 244906 (2014).
 - [12] M. E. Cates and E. Tjhung, *J. Fluid Mech.* **836**, P1 (2018).
 - [13] I. M. Lifshitz and V. V. Slyozov, *J. Phys. Chem. Solids* **19**, 35 (1961).
 - [14] C. Wagner, *Z. Electrochem.* **65**, 581 (1961).
 - [15] P. Voorhees, *Annu. Rev. Mater. Sci.* **22**, 197 (1992).
 - [16] D. A. Huse, *Phys. Rev. B* **34**, 7845 (1986).
 - [17] J. G. Amar, F. E. Sullivan, and R. D. Mountain, *Phys. Rev. B* **37**, 196 (1988).
 - [18] J. F. Marko and G. T. Barkema, *Phys. Rev. E* **52**, 2522 (1995).
 - [19] D. W. Heermann, L. Yixue, and K. Binder, *Phys. A (Amsterdam)* **230**, 132 (1996).
 - [20] K. Binder and D. Stauffer, *Phys. Rev. Lett.* **33**, 1006 (1974).
 - [21] K. Binder, *Phys. Rev. B* **15**, 4425 (1977).
 - [22] E. D. Siggia, *Phys. Rev. A* **20**, 595 (1979).
 - [23] H. Furukawa, *Phys. Rev. A* **31**, 1103 (1985).
 - [24] H. Furukawa, *Phys. Rev. A* **36**, 2288 (1987).
 - [25] M. San Miguel, M. Grant, and J. D. Gunton, *Phys. Rev. A* **31**, 1001 (1985).
 - [26] J. E. Farrell and O. T. Valls, *Phys. Rev. B* **43**, 630 (1991).
 - [27] A. Shinozaki and Y. Oono, *Phys. Rev. E* **48**, 2622 (1993).
 - [28] T. Koga and K. Kawasaki, *Phys. A (Amsterdam)* **196**, 389 (1993).
 - [29] H. Tanaka, *Phys. Rev. Lett.* **72**, 1702 (1994).
 - [30] H. Tanaka, *J. Chem. Phys.* **103**, 2361 (1995).
 - [31] H. Tanaka, *J. Chem. Phys.* **105**, 10099 (1996).
 - [32] M. Laradji, S. Toxvaerd, and O. G. Mouritsen, *Phys. Rev. Lett.* **77**, 2253 (1996).
 - [33] H. Tanaka, *J. Chem. Phys.* **107**, 3734 (1997).
 - [34] S. Bastea and J. L. Lebowitz, *Phys. Rev. Lett.* **78**, 3499 (1997).
 - [35] V. M. Kendon, M. E. Cates, I. Pagonabarraga, J. C. Desplat, and P. Blandon, *J. Fluid Mech.* **440**, 147 (2001).
 - [36] C. Datt, S. P. Thampi, and R. Govindarajan, *Phys. Rev. E* **91**, 010101(R) (2015).
 - [37] S. Majumder and S. K. Das, *Europhys. Lett.* **95**, 46002 (2011).
 - [38] S. Roy and S. K. Das, *Soft Matter* **9**, 4178 (2013).
 - [39] R. Shimizu and H. Tanaka, *Nat. Commun.* **6**, 7407 (2015).
 - [40] A. K. Thakre, W. K. den Otter, and W. J. Briels, *Phys. Rev. E* **77**, 011503 (2008).
 - [41] H. Kabrede and R. Hentschke, *Phys. A (Amsterdam)* **361**, 485 (2006).
 - [42] S. W. Koch, R. C. Desai, and F. F. Abraham, *Phys. Rev. A* **27**, 2152 (1983).

- [43] V. Kumaran, *J. Chem. Phys.* **109**, 7644 (1998).
- [44] J.-P. Hansen and I. R. McDonald, *Theory of Simple Liquids* (Academic, London, 2008).
- [45] S. K. Das, J. V. Sengers, and M. E. Fisher, *J. Chem. Phys.* **127**, 144506 (2007).
- [46] T. M. Squires and J. F. Brady, *Phys. Fluids* **17**, 073101 (2005).
- [47] D. Frenkel and B. Smit, *Understanding Molecular Simulations: From Algorithms to Applications* (Academic, San Diego, 2002).
- [48] M. P. Allen and D. J. Tildesly, *Computer Simulations of Liquids* (Clarendon, Oxford, 1987).
- [49] S. Roy and S. K. Das, *J. Chem. Phys.* **139**, 044911 (2013).
- [50] S. Nosé, *J. Chem. Phys.* **81**, 511 (1984).
- [51] W. G. Hoover, *Phys. Rev. A* **31**, 1695 (1985).
- [52] W. G. Hoover, *Studies in Modern Thermodynamics* (Elsevier, New York, 1991).
- [53] S. K. Das, J. Horbach, K. Binder, M. E. Fisher, and J. V. Sengers, *J. Chem. Phys.* **125**, 024506 (2006).
- [54] S. Roy and S. K. Das, *Europhys. Lett.* **94**, 36001 (2011).
- [55] D. P. Landau and K. Binder, *A Guide to Monte Carlo Simulations in Statistical Physics* (Cambridge University Press, Cambridge, 2009).
- [56] H. C. Andersen, *J. Chem. Phys.* **72**, 2384 (1980).
- [57] S. Roy and S. K. Das, *Eur. Phys. J. E* **38**, 132 (2015).
- [58] J. Hoshen and R. Kopelman, *Phys. Rev. B* **14**, 3438 (1976).
- [59] S. Paul and S. K. Das, *Phys. Rev. E* **96**, 012105 (2017).
- [60] C. Yeung, *Phys. Rev. Lett.* **61**, 1135 (1988).
- [61] G. Porod, *Small-Angle X-Ray Scattering*, edited by O. Glatter and O. Kratky (Academic, New York, 1982).
- [62] Y. Oono and S. Puri, *Mod. Phys. Lett. B* **02**, 861 (1988).
- [63] A. J. Bray and S. Puri, *Phys. Rev. Lett.* **67**, 2670 (1991).
- [64] P. C. Hohenberg and B. I. Halperin, *Rev. Mod. Phys.* **49**, 435 (1977).
- [65] K. Binder, *Phys. Rev. A* **29**, 341 (1984).
- [66] S. K. Das, J. Horbach, and K. Binder, *Phase Transitions* **77**, 823 (2004).
- [67] S. Plimpton, *J. Comput. Phys.* **117**, 1 (1995).
- [68] <https://www.lammps.org/#gsc.tab=0>.